

Numerical study of the Eulerian-Lagrangian formulation of the Navier-Stokes equations

K. Ohkitani

*Research Institute for Mathematical Sciences,
Kyoto University, Kyoto 606-8502 Japan**

P. Constantin

*Department of Mathematics,
The University of Chicago
Chicago, Il 60637, USA*

(Dated: June 21, 2003)

Abstract

An Euler-Lagrangian analysis of the Navier-Stokes equations is performed with use of numerical simulations. On this basis we propose a new method for capturing vortex reconnection. It is found that the diffusive Lagrangian map becomes non-invertible under time evolution and requires resetting for its calculation. This sets a time scale and its frequent resetting corresponds to vortex reconnection. Another time scale defined by the connection coefficients, responsible for non-commutativity of Euler and Euler-Lagrange derivatives, is shown to be on the same order during reconnection. This introduces a novel singular perturbation problem of connection anomaly underlying reconnection.

PACS numbers: 47.27.AK, 47.10.+g

*Electronic address: ohkitani@kurims.kyoto-u.ac.jp

The Euler equations, a totally inviscid form of the Navier-Stokes equations, are known to possess a number of inviscid invariants. In particular it is well known that the vortex lines are frozen in fluids. Topological change (reconnection) is not possible in smooth solutions of the inviscid flow, but is possible in the presence of viscosity. Recently, a framework of the Navier-Stokes equations that is suitable for the study of topological properties of vortex lines in viscous flow has been developed by one of the authors [1–3].

This Eulerian-Lagrangian framework is based on a generalization of Weber’s transform (see Eqs.(3),(4) below) to viscous fluid. It incorporates nonlocal interaction and viscous diffusion in a multiplicative fashion. This formalism has been developed for the analytical Navier-Stokes theory [1–3]. Nevertheless, with purely analytical methods it is difficult to analyze long time evolution of the Navier-Stokes equations under which vortex reconnection actually takes place.

We present here results of an Eulerian-Lagrangian analysis using numerical simulations of the Navier-Stokes equations. The question we raise here is to ask whether or not this Eulerian-Lagrangian formalism captures vortex reconnection successfully, and if yes how. More specifically, the purposes of this paper are i) to search for characteristic time scales associated with vortex reconnection in this formalism and ii) to give them a dynamical significance. A novel kind of singular perturbation problem is associated with ii), which can cover broader class of physical problems such as fast reconnection in magneto-hydrodynamics.

The Navier-Stokes equations and the continuity equation read

$$\frac{\partial \mathbf{u}}{\partial t} + (\mathbf{u} \cdot \nabla) \mathbf{u} = -\nabla p + \nu \Delta \mathbf{u}, \quad (1)$$

and $\text{div } \mathbf{u} = 0$ where with standard notation \mathbf{u} for velocity, p pressure and ν for kinematic viscosity. Using another dependent variable called impulse \mathbf{w} , which is not incompressible in

general, we may alternatively describe time evolution of the flow by the following equations

$$\frac{\partial \mathbf{w}}{\partial t} + (\mathbf{u} \cdot \nabla) \mathbf{w} = -(\nabla \mathbf{u})^T \mathbf{w} + \nu \Delta \mathbf{w}, \quad (2)$$

where T denotes matrix transpose. The usual incompressible velocity \mathbf{u} is obtained by solenoidal projection \mathbf{P} of \mathbf{w}

$$\mathbf{u} = \mathbf{P}(\mathbf{w}). \quad (3)$$

This formalism is sometimes referred to as the impulse formalism [4]. (See also [6, 7] for its application boundary layer flows).

It should be noted that \mathbf{w} can be represented in a multiplicative fashion as follows

$$\mathbf{w} = (\nabla A)^T \mathbf{v}. \quad (4)$$

In this decomposition, \mathbf{A} denotes the diffusive Lagrangian label and \mathbf{v} the virtual velocity, which obey the following equations [1]

$$\frac{\partial \mathbf{A}}{\partial t} + (\mathbf{u} \cdot \nabla) \mathbf{A} = \nu \Delta \mathbf{A}, \quad (5)$$

and

$$\frac{\partial \mathbf{v}}{\partial t} + (\mathbf{u} \cdot \nabla) \mathbf{v} = 2\nu \mathbf{C} : \nabla \mathbf{v}, \quad (6)$$

where the i -th component of $\mathbf{C} : \nabla \mathbf{v}$ is $C_{m,k;i} \frac{\partial v_m}{\partial x_k}$ and $C_{m,k;i} = \frac{\partial x_j}{\partial A_i} \frac{\partial^2 A_m}{\partial x_j \partial x_k}$. It is important to bear in mind that \mathbf{C} measures non-commutativity between the Euler and Euler-Lagrange derivatives; $[\nabla_A^i, \nabla_E^k] = C_{m,k;i} \nabla_A^m$. On top of $\boldsymbol{\omega}(\mathbf{x}, t) = \nabla \times \mathbf{u}(\mathbf{x}, t)$ we define virtual vorticity by $\boldsymbol{\zeta}(\mathbf{x}, t) = \nabla_A \times \mathbf{v}(\mathbf{x}, t)$. Equations (3,4,5,6) form a closed system which is equivalent to the Navier-Stokes equations. We note that derivatives with respect to \mathbf{A} are defined using $(\nabla \mathbf{A})^{-1}$, see [1-3] for details.

Two technical points of the numerical method that should be mentioned are as follows. As a basic equation, we have rewritten (2) as

$$\frac{\partial \mathbf{w}}{\partial t} = -\nabla(\mathbf{w} \cdot \mathbf{u}) + \mathbf{u} \times \boldsymbol{\omega} + \nu \Delta \mathbf{w}, \quad (7)$$

because fast Fourier transforms can be implemented efficiently this way. Another aspect is that it is not easy to evolve \mathbf{v} because \mathbf{C} , a cubic quantity in \mathbf{A} , is cumbersome to handle. Instead of dealing with \mathbf{v} directly, we have solved for displacement vector $\boldsymbol{\ell} = \mathbf{A} - \mathbf{x}$. It satisfies a passive equation

$$\frac{\partial \boldsymbol{\ell}}{\partial t} + (\mathbf{u} \cdot \nabla) \boldsymbol{\ell} = -\mathbf{u} + \nu \Delta \boldsymbol{\ell}. \quad (8)$$

Once $\boldsymbol{\ell}$ is obtained, the connection coefficients \mathbf{C} and all other quantities of interest can be obtained *a posteriori* by matrix inversion. In practice, we have solved (7) and (8) simultaneously. A 2/3-dealiased pseudo-spectral method was employed under periodic boundary conditions. The grid points used were 128^3 and 256^3 . Time marching was performed with a fourth-order Runge-Kutta scheme.

We have chosen an initial condition of two orthogonally placed vortex tubes, which was examined numerically to study in detail vortex reconnection with conventional methods of analysis [9]. At the Reynolds numbers covered here the physics is not new, but we intend to give a novel diagnosis of it by the Eulerian-Lagrangian formalism.

Once $\boldsymbol{\ell}$ is known we can compute $\nabla \mathbf{A}$ by $\frac{\partial A_i}{\partial x_j} = \frac{\partial \ell_i}{\partial x_j} + \delta_{ij}$. In inviscid fluids the determinant of $\nabla \mathbf{A}$ is constant and its invertibility is maintained automatically under time evolution. In the case of viscous fluids the determinant is not preserved in general [1]. Therefore it is possible that it becomes zero and the matrix can become non-invertible under time evolution of the Navier-Stokes equations. Indeed, according to our numerical simulation, this actually takes place. In order to ensure the invertibility it is necessary to reset $\boldsymbol{\ell} = 0$ when the determinant becomes very small. Practically we reset $\boldsymbol{\ell}$ if $|\det(\nabla \mathbf{A})| \leq \epsilon$, where ϵ is a preassigned small parameter. Since the equation for $\boldsymbol{\ell}$ is passive, the resetting procedure does not affect the evolution of \mathbf{u} . Also, it has been shown that properties of $\boldsymbol{\ell}$ are independent from ϵ (See [3]).

The values of viscosity chosen are $\nu = 4 \times 10^{-3}$ for 256^3 grid (Case 1) $\nu = 1 \times 10^{-2}$ for

128³ grid (Case 2). It turned out that for an accurate calculation of \mathbf{C} we need to make the Reynolds number lower than commonly adopted to ensure the accuracy of velocity and vorticity. More precisely, $k_{\max}/k_d \geq 1.4$ may be sufficient for resolving $\boldsymbol{\omega}$, but not for \mathbf{C} . In all the calculations presented here we have $k_{\max}/k_d \geq 2$ which ensures accuracy of both $\boldsymbol{\omega}$ and \mathbf{C} . Here k_{\max} is the maximum wavenumber and k_d is the Kolmogorov dissipative wavenumber.

In Fig.1(a) we show the time evolution of enstrophy $Q(t) \equiv \frac{1}{2} \langle |\boldsymbol{\omega}|^2 \rangle$ and virtual-enstrophy $Q_\zeta(t) \equiv \frac{1}{2} \langle |\boldsymbol{\zeta}|^2 \rangle$ for the two different values of viscosity. Here $\langle \ \rangle$ denotes a spatial average over $[0, 2\pi]^3$. With $\nu = 4 \times 10^{-3}$ the enstrophy increases in time and attains its maximum around $t = 9.0$, whereas with $\nu = 1 \times 10^{-2}$ it basically decreases with time monotonically. In the latter case, viscosity is too large for intense vortex stretching to take place. In both cases the virtual-enstrophy basically tracks the enstrophy well because of frequent resetting. The enstrophy is larger than the virtual-enstrophy for most of the time. It should be noted however that this is not always true, e.g. $t = 3.0$ for the Case 2.

In Fig.1(b) time evolution of $\max |\boldsymbol{\omega}|$ is compared with that of $\max |\boldsymbol{\zeta}|$ for Case 1. As in Fig.1(a) they are tracking with each other. These local quantities show strong peaks between $t = 3.5$ and 5 [9]. During this time interval vortex reconnection is taking place (see below). Plots for Case 2 is similar to Fig.1(a), except that the peak value is smaller by a factor of about 50 (figure omitted).

Iso-surface plots of $|\boldsymbol{\omega}|$ and $|\boldsymbol{\zeta}|$ at time $t = 3$ are shown in Fig.2. This is the time two vortex tubes begin to form bridges. A more careful examination reveals that there is no big difference between $|\boldsymbol{\omega}|$ and $|\boldsymbol{\zeta}|$, although the bridges are more prominent in $|\boldsymbol{\omega}|$ than in $|\boldsymbol{\zeta}|$.

In Fig.3(a) the time evolution of the mean square displacement $E_\ell(t) = \frac{1}{2} \langle |\boldsymbol{\ell}|^2 \rangle$ is shown for Cases 1 and 2. The threshold is chosen as $\epsilon = 0.01$. We have checked that the frequent resetting occurs at the same time interval with $\epsilon = 0.1, 0.001$. In view of an iden-

tity $d\text{vol}(\mathbf{A}) = \det(\nabla \mathbf{A}) d\text{vol}(\mathbf{x})$ ($d\text{vol}$ =a volume element in each space), the vanishing of $\det(\nabla \mathbf{A})$ is interpreted roughly as unusually intense particle diffusion, connecting infinitesimal \mathbf{A} -element with finite \mathbf{x} -element. In the early stage $t \leq 1.5$ the difference is small between the two cases. After that, a significant difference is seen between the two cases. The resetting interval is smaller in Case 1 than Case 2. Correspondingly the magnitude is larger in Case 2 than in Case 1. In both cases, resetting procedure becomes very frequent around the interval $3.5 \leq t \leq 5$, during vortex reconnection (see below).

In order to extract the time scale associated with the resetting more quantitatively, we define the resetting intervals $\Delta t_j = t_j - t_{j-1}$, for $j = 1, 2, \dots$ where $0 < t_1 < t_2 < \dots$ are times at which resetting occurs. In Fig.3(b) the time intervals of resetting are shown. For Case 1 there are two dips of time intervals at $t = 4$ and $t = 9$. The former corresponds to vortex reconnection and the latter to the maximum of total enstrophy. Resetting occurs quite frequently around these times and the time scale is $0.05 < \Delta t < 0.1$. For Case 2, a dip around $t = 4.5$ is also noticeable with a time scale of about 0.2. It is interesting to note that more frequent resettings occur with a smaller value of viscosity, reflecting that vortex reconnection is not a purely viscous phenomenon.

It may be in order to compare the above findings with those described in [9]. There, the start of vortex reconnection is defined as the time when two vortices form a local dipole at $t \approx 3$. The jet velocity associated with the dipole attains maximum at $t \approx 3.6$ (formation of bridge). The vorticity attains a maximum at $t \approx 4.3$ (formation of new topology). The local maximum is no longer located in the remnant contact zone at $t \approx 5.2$. It should be noted that the very frequent resetting takes place between the formation of bridge and that of new topology. This suggests that the present method captures cut-and-connect type reconnection successfully.

Now, we consider the connection coefficients \mathbf{C} which control the viscous effect on the

evolution of \mathbf{v} . They are related with the curvature of particle trajectories in the flow. Noting that \mathbf{C} has a dimension of inverse length, we may form an inverse time scale as $(\tau_{\mathbf{C}})^{-1} = \frac{\nu}{27}(\max_{\mathbf{x}} |\mathbf{C}|)^2$. Here $|\mathbf{C}|^2 = C_{m,k;i}C_{m,k;i}$ and the prefactor $1/27$ comes from the number of components of \mathbf{C} . The inverse time scale $(\tau_{\mathbf{C}})^{-1}$ was examined for the two cases (figure omitted). It fluctuates violently in time, ranging from 0.01 to 100. It is difficult to tell when reconnection happens by solely looking at it. Nevertheless, around $t = 4$ and 5, $\tau_{\mathbf{C}} \approx 0.1$, which is on the order of resetting time interval found above. It should be noted that $(\tau_{\mathbf{C}})^{-1}$ fluctuates around $O(1)$, in spite of a small value of viscosity. This suggests a new phenomenon of connection anomaly, i.e. finiteness of $\nu \sup_{\mathbf{x}, t_0, \delta t} \int_{t_0}^{t_0 + \delta t} |\mathbf{C}|^2 dt$ when $\nu \rightarrow 0$ is underlying the reconnection process. It is similar to dissipation anomaly (i.e. finite energy dissipation when $\nu \rightarrow 0$), a key issue in turbulence.

We note that the reciprocal Kolmogorov time scale $(\tau_{k_d})^{-1} = \sqrt{\epsilon_{\text{dis}}/\nu} = \sqrt{2Q(t)} \approx 4$, that is, $\tau_{k_d} \approx 0.25$ at $t = 4$ for Case 1, where ϵ_{dis} is the total dissipation rate of energy. It should be noted that this time scale, formed from the total enstrophy, is comparable to, but smaller than $(\tau_{\mathbf{C}})^{-1}$ at $t = 4$. To summarize, during the reconnection we have $\Delta t \leq \tau_{\mathbf{C}} < \tau_{k_d}$.

Finally, we show the iso-surface plots of $|\mathbf{C}|$ in Fig.4. The regions with high $|\mathbf{C}|$ form layer-like structures, surrounding the vortex tubes. This shows that particle trajectories undergo strong deformation in ambient region around vortex tubes.

We have numerically identified two time scales relevant to vortex reconnection in this formalism; one is the resetting time scale and the other one is connected with anomaly of the connection coefficients. It is found that the first time scale correctly captures vortex reconnection and the second is on the same order during vortex reconnection, suggesting that connection anomaly is underlying reconnection. In summary, this method provides not only an automated identification of reconnection but also a dynamical significance to it by

extracting a novel singular perturbation problem.

The present method has been applied to a 2D MHD problem, where magnetic reconnection is captured successfully by frequent resetting. It has also been applied to the problem of the Taylor-Green vortex [10]. In this flow vortex layers are formed in the early stage, followed by their rolling-up by Kelvin-Helmholtz instability, a process where cut-and-connect type reconnection is absent. Consistently, no resetting has been observed during the disintegration of these layers. This shows that the present method distinguishes vortex reconnection from other effects of vorticity diffusion. These results will be reported elsewhere. Detailed comparison with previous studies [11–13] will be also of reported in future.

Acknowledgments

One of the authors (K.O.) would like to thank R. Pelz for helpful comments. This work was started when one of the authors (P.C.) visited Research Institute for Mathematical Sciences, Kyoto University in October 2001 on an invitation fellowship by Japan Society for the Promotion of Science. This work has been supported by Grant-in-Aid for scientific research from the Ministry of Education, Culture, Sports, Science and Technology of Japan, under Nos. 14540203 and 14204007.

-
- [1] P. Constantin, "An Eulererian-Lagrangian Approach to the Navier-Stoks Equations," *Commun. Math. Phys.* **216**, 663(2001).
 - [2] P. Constantin, "An Eulererian-Lagrangian Approach for incompressible fluids: local theory," *J. Amer. Math. Soc.* **14** 263(2001).
 - [3] P. Constantin, to appear in *Handbook of Mathematical Fluid Dynamics, Volume 2*, S. Friedlander, D. Serre, eds, Elsevier.
 - [4] G. Russo and P. Smerka, "Impulse formulation of the Euler equations: General properties and numerical methods," *J. Fluid Mech.* **391**, 189(1999).

- [5] W. E and J.-G. Liu, “Finite difference schemes for incompressible flows in the velocity-impulse density formulation,” *J. Comput. Phys.* **130**, 67(1997).
- [6] D.M. Summers, “On the formation of vortices at a solid boundary ,” *Proc. Roy. Soc. Lond. A* **456**, 1183(2000).
- [7] D.M. Summers, “Towards an impulse-based Lagrangian model of boundary layer turbulence,” *Physica D* **154**, 287(2002).
- [8] It was reported in [5] that a numerical scheme based on (2) is unstable. It was checked that a conventional numerical solution of the Navier-Stokes equations give the identical result with that of (2), as far as the current initial condition and the Reynolds numbers are concerned.
- [9] O.N. Boratav, R.B. Pelz & N.J. Zabusky, “Reconnection in orthogonally interacting vortex tubes: Direct numerical simulations and quantifications,” *Phys. Fluids A* **4**581(1992).
- [10] M. Brachet *et al.*, “Small-scale structure of the Taylor-Green vortex,” *J. Fluid Mech.* **130**, 411(1983).
- [11] S. Kida and M. Takaoka, “Vortex reconnection,” *Annu. Rev. Fluid Mech.* **26**, 169(1994).
- [12] M.V. Melander and F. Hussain, “Topological vortex dynamics in axisymmetric viscous flows,” *J. Fluid Mech.* **260**, 57(1994).
- [13] M.G. Linton, R.B. Dahlburg and S.K. Antiochos, “Reconnection of twisted flux tubes as a function of contact angle,” *Astrophys. J.* **553**, 905(2001).

Figure captions

- Fig.1: Time evolution of (a) enstrophy and virtual-enstrophy and of (b) $\max|\boldsymbol{\omega}|$ (solid line) and $\max|\boldsymbol{\zeta}|$ (dashed line) for Case 1. In (a), $Q(t)$ and $Q_\zeta(t)$ are denoted by a solid line and circles for case 1 and by dashed line and squares for case 2.
- Fig.2: Iso-surfaces plots of $|\boldsymbol{\omega}|$ (darker gray) and $|\boldsymbol{\zeta}|$ (lighter gray) at $t = 3$ for Case 1.
- Fig.3: Time evolution of (a) the spatial average $E_\ell(t)$ of the displacement and of (b) time intervals of resetting Δt_j against t_j . Case 1 is denoted by a solid line and Case 2 by a dashed line.
- Fig.4: Iso-surfaces plots of $|\boldsymbol{\omega}|$ (darker gray) and $|C|$ (lighter gray) at $t = 3$ for Case 1.

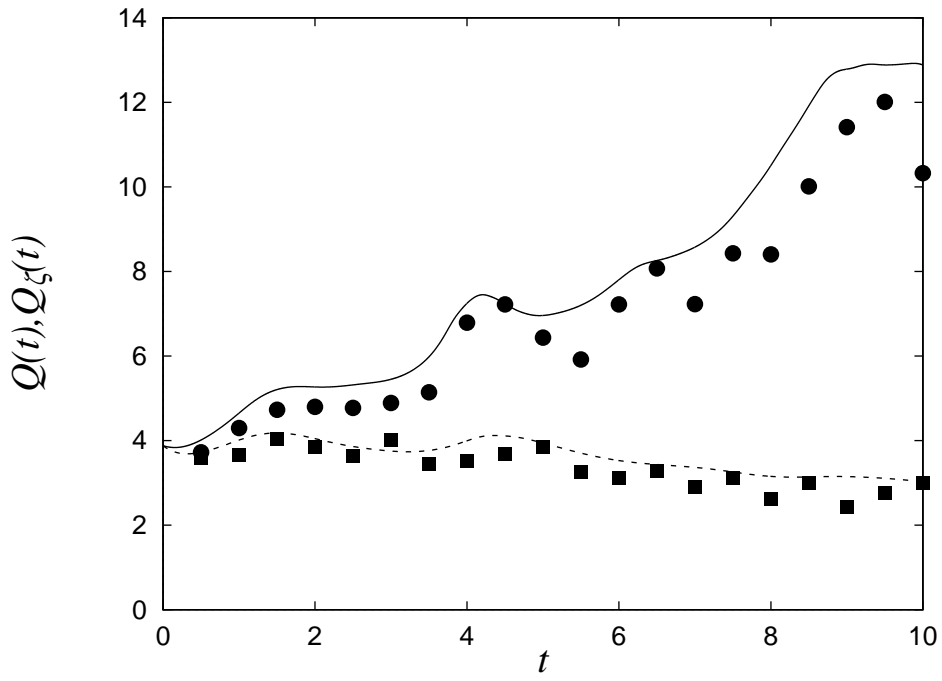


Fig.1(a), Ohkitani, Physics of Fluids

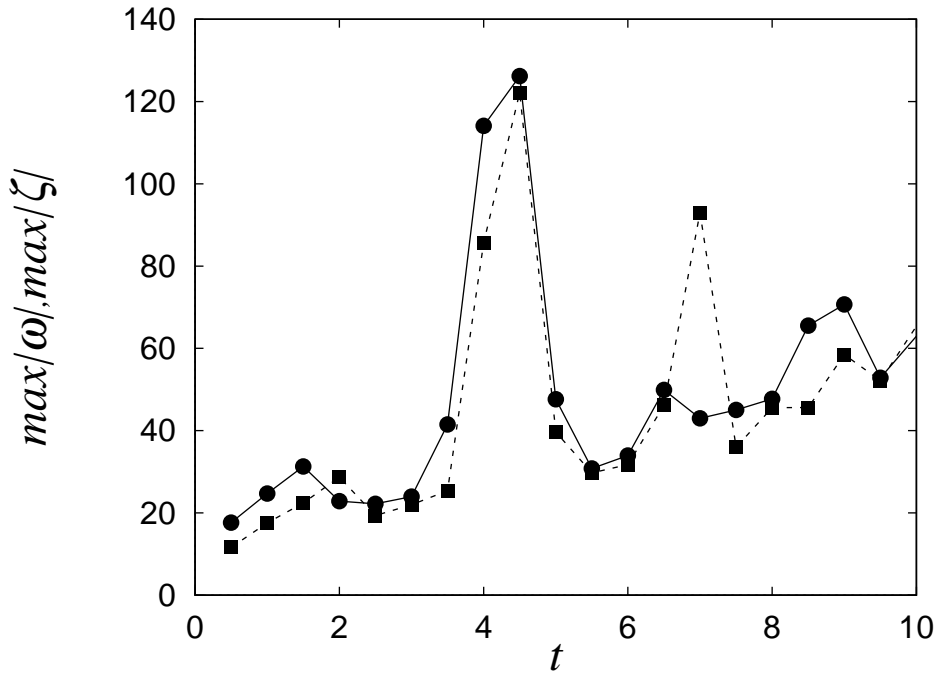


Fig.1(b), Ohkitani, Physics of Fluids

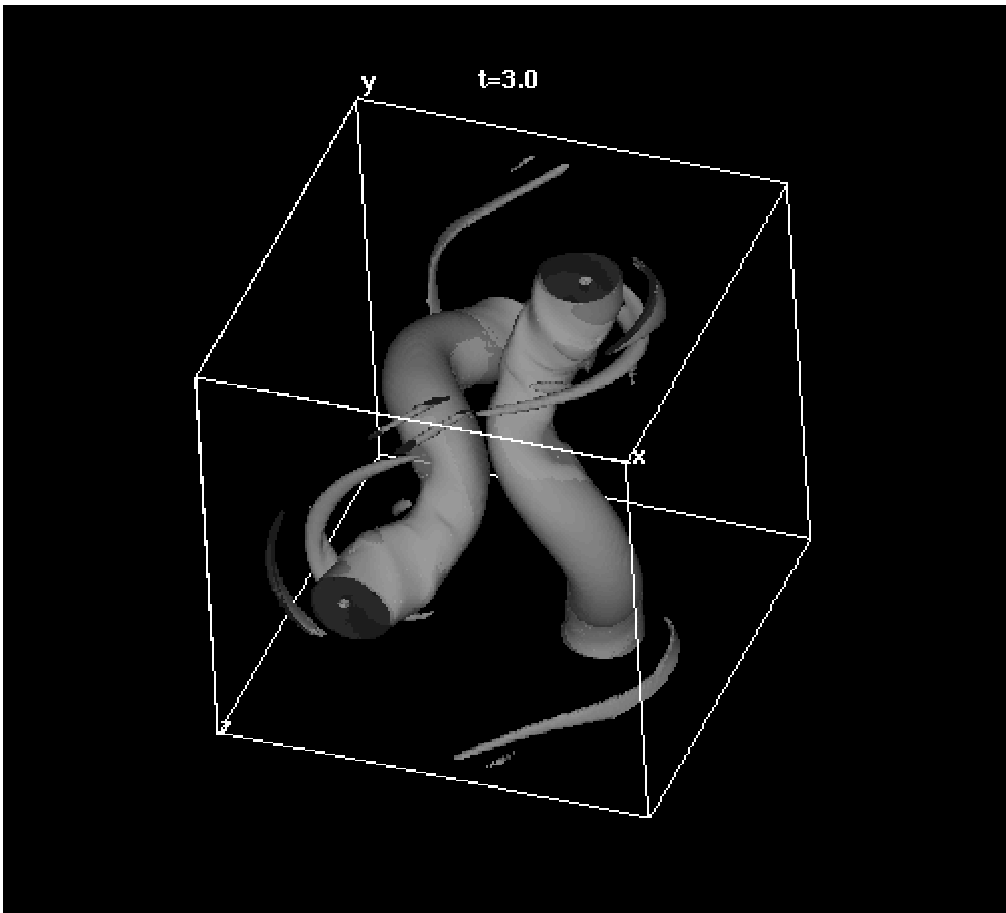


Fig.2, Ohkitani, Physics of Fluids

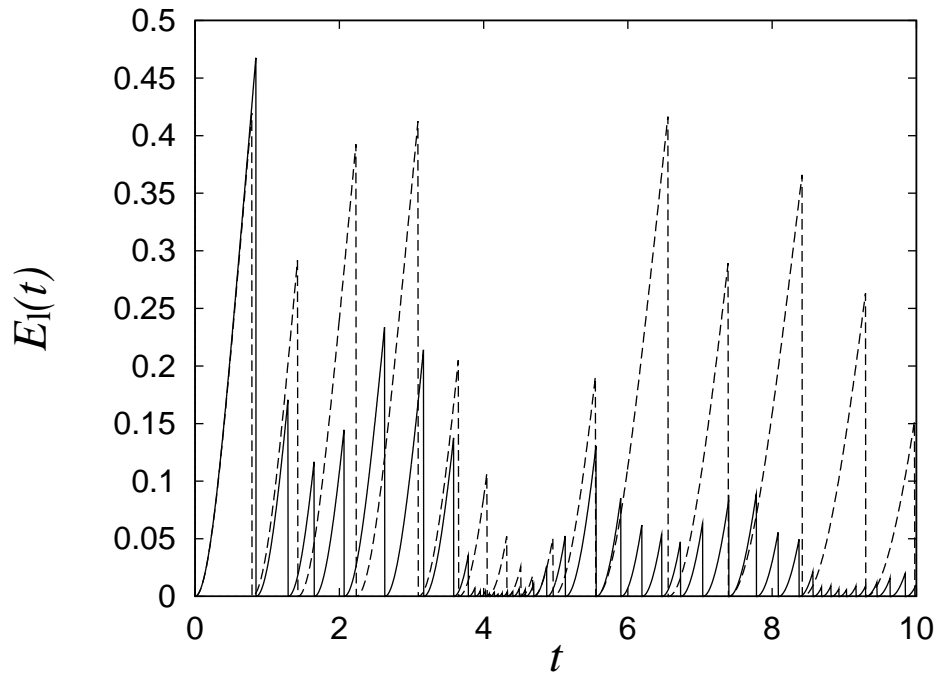


Fig.3(a), Ohkitani, Physics of Fluids

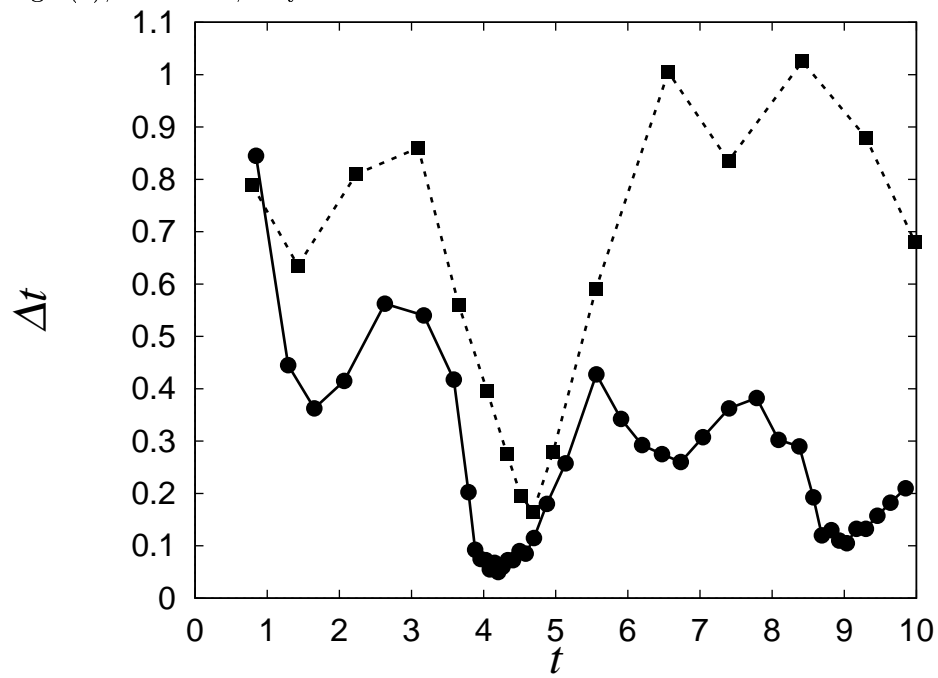


Fig.3(b), Ohkitani, Physics of Fluids

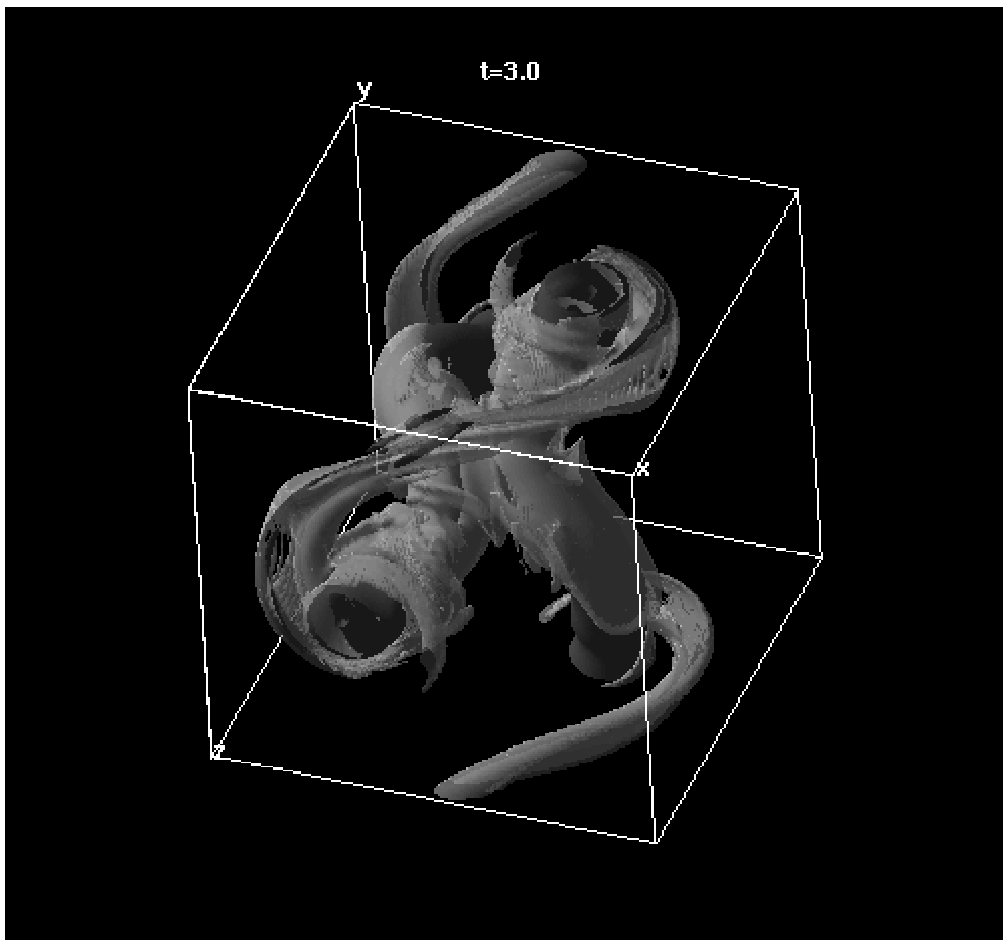


Fig.4, Ohkitani, Physics of Fluids